

Research Paper

Ascorbic acid induced HepG2 cells' apoptosis via intracellular reductive stress

Xiaonan Gao^{*}, Keyan Wei^{*}, Bo Hu, Kehua Xu[✉], Bo Tang[✉]

College of Chemistry, Chemical Engineering and Materials Science, Collaborative Innovation Center of Functionalized Probes for Chemical Imaging in Universities of Shandong, Key Laboratory of Molecular and Nano Probes, Ministry of Education, Shandong Provincial Key Laboratory of Clean Production of Fine Chemicals, Shandong Normal University, Jinan 250014, P. R. China

^{*}X. Gao and K. Wei contributed equally to this work.

✉ Corresponding authors: Xukehua@sdsu.edu.cn (Kehua Xu); Tangb@sdsu.edu.cn (Bo Tang)

© Ivyspring International Publisher. This is an open access article distributed under the terms of the Creative Commons Attribution (CC BY-NC) license (<https://creativecommons.org/licenses/by-nc/4.0/>). See <http://ivyspring.com/terms> for full terms and conditions.

Received: 2019.02.02; Accepted: 2019.05.07; Published: 2019.05.31

Abstract

Goals: Destruction of the redox balance in tumor cells is of great significance for triggering their apoptosis in clinical applications. We designed a pH sensitive multifunctional drug nanocarrier with controllable release of ascorbic acid under hypoxic environment to induce tumor cells' apoptosis via enhancing reductive stress, thereby dealing minimum damage to normal tissues.

Methods: A core-shell nanostructure of CdTe quantum dots with mesoporous silica coating was developed and functionalized with poly(2-vinylpyridine)-polyethylene glycol-folic acid, which achieves cancer cells' targeting delivery and reversibly pH controlled release of ascorbic acid both *in vitro* and *in vivo*.

Results: The result demonstrated that ascorbic acid can indeed lead liver cancer cells' death with the increase of nicotinamide adenine dinucleotide phosphate, while normal cells not being affected. The molecular mechanism of apoptosis induced by ascorbic acid was firstly elucidated at cellular levels, and further confirmed *via in vivo* investigations.

Conclusion: For the first time we proposed the concept for applying reductive stress into cancer treatments, which brings great advantage of toxicity free and less damage to normal tissues. In general, this technique has taken an important step in the development of a targeted tumor treatment system, providing perspectives for the design of medicines *via* reductive stress, and offers new insights into future clinical mild-therapies.

Key words: Ascorbic Acid, pH Control, Nanocarrier, Reductive Stress, Mild-therapy

Introduction

Liver cancer, as one of the most common malignant tumors, has brought severe challenges on the clinical treatments due to their insensitivity to chemotherapy and poor prognosis [1]. Up to date, surgery, radiotherapy and chemotherapy are the most common methods for curing cancer, but are still limited by critical side effects [2]. In the past decade, research interest has been focused on oxidative damage to tumors, thereby leads to their apoptosis by oxidative stress. However, it was recently proved that oxidative stress also brings inevitable damage to normal organs and tissues as well, which makes it

currently the insurmountable bottleneck in clinical treatments [3-5]. Therefore, as tumor environment has high levels of reducing components, such as glutathione, nicotinamide adenine dinucleotide phosphate (NADPH) and nitroreductas [6-11], reductive stress, the other imbalance form in redox balance [12, 13], is hypothesized to induce tumor cell apoptosis by further enhance the redox imbalance [14], while dealing less damage to normal cells [15-17].

In this regard, ascorbic acid (AA), an essential nutrient for human growth and physiological health, serves as an optimal reducing agent in human fluids

[18, 19] for removing active oxygen groups and free radicals [20-23]. Not like Vitamin E that works as an antioxidant at the cellular level, low transmembrane efficiency of AA critically limits its antioxidative function within the cells [24]. In previous reports, high-dose AA (4 g/kg) exhibits decent antitumor efficiency, as it is firstly oxidized to dehydroascorbic acid (DHA) for entering into the cell, and then rises reactive oxygen species to trigger oxidative stress, resulting in tumor cells' apoptosis [25]. However, how to use the reducing environment of tumor cells to further strengthen the degrees of reducing stress by introducing AA into the cells, while resulting in tumor cells' apoptosis but normal cells not being affected, is of great research significance [26-28].

Herein, a core-shell nanostructure of CdTe quantum dots with mesoporous silica (MSN) coating was synthesized [29-33], and functionalized with poly(2-vinylpyridine)-polyethylene glycol-folic acid (PPF) [34] for reversibly pH controlled releasing AA in targeted liver cancer cells (Scheme 1). Since the CdTe quantum dots' fluorescence recovers after AA released from the nanocarrier, the fluorescence intensity change acts as a promising indicator for the treatment. For the first time we discovered that reductive stress under hypoxic conditions *via* AA triggers HepG2 cells' apoptosis, exploring a possible approach with advantages of cost-effective, low toxicity and minimum side effect. Therefore, such drug delivery method and new mechanism for inducing cancer cells' apoptosis are expected to establish a theoretical system of "mild treatment" in the future.

Results and Discussion

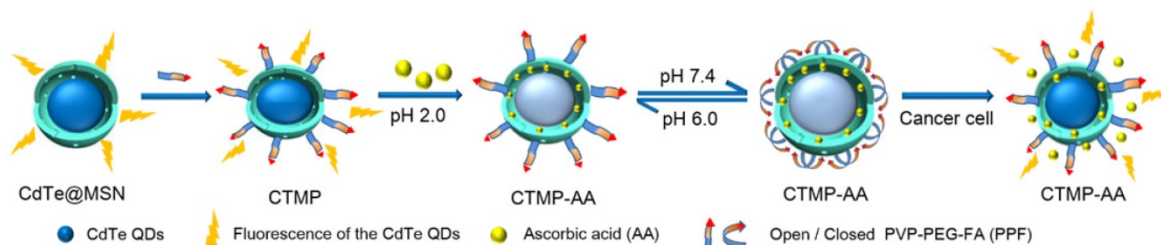
Preparation and Characterization of CTMP

The nanocarrier was synthesized following typical previous literature with further modification [35, 36], and characterized by transmission electronic microscopy (TEM), UV-visible absorption spectroscopy (UV-Vis) and fluorescence spectroscopy. According to Figure 1A, the TEM image displays a smooth spherical shape for the CdTe@MSN, and an average size of 70 ± 5 nm. After binding with PPF

(Figure S1) to form the CdTe@MSN@PPF (CTMP), the particle sizes increased to 90 ± 8 nm, as the coating of the polymers completely encapsulated the CdTe@MSN (Figure 1B). Such kind of encapsulation could prevent the leakage of the loaded drug, and also increase the targeting effect of the nanocarriers to the overexpressed folic acid receptor in tumor cell membranes. The BET surface area analysis on the CdTe@MSN nanoparticles and CTMP was carried out to analyze the pore diameter change. As can be seen from Figure S2, the pores in the CdTe@MSN nanoparticles are mainly distributed in the mesopore and macropore range (Figure S2A), which are contributed by the mesoporous structure of MSN coating. After PPF functionalization, the pores were blocked by tuning the pH, thereby increasing the number of micropores (Figure S2B). From the fluorescence spectra (Figure 1C), the maximum emission wavelength of the CdTe@MSN and CTMP both were obtained at 548 nm. Compared with CdTe@MSN, the blue shift of the maximum absorption peak position (Figure S3) indicates that the surface state changed after the polymer functionalization of PPF, which attributes to the change of surface/volume ratio for the nanocarriers. Therefore, we expect that the nanocarriers with fluorescent properties will be an ideal candidate for both *in vitro* labeling and *in vivo* deep tissue imaging.

Drug loading and release

AA was chosen as the drug for the investigation of the uptake and release from CTMP-AA. The loading capacity of AA on the CTMP was calculated to be 47 ± 2 $\mu\text{g}/\text{mg}$ according to the standard linear calibration curve (Figure S4). Afterwards, the high resolution mass spectrometry (HRMS) was used to detect AA which released from CTMP-AA in sodium citrate buffer solution (pH = 6.0), and the negative ion peak of AA was obtained at 175.0254 (Figure S5), which is consistent with the molecular formula of AA. These results demonstrate that the as prepared nanocarriers CTMP-AA prevent AA from being oxidized to DHA before releasing, which is helpful for the AA's *in vivo* study.



Scheme 1. Schematic illustration for the synthesis process of the nanocarrier CTMP-AA.

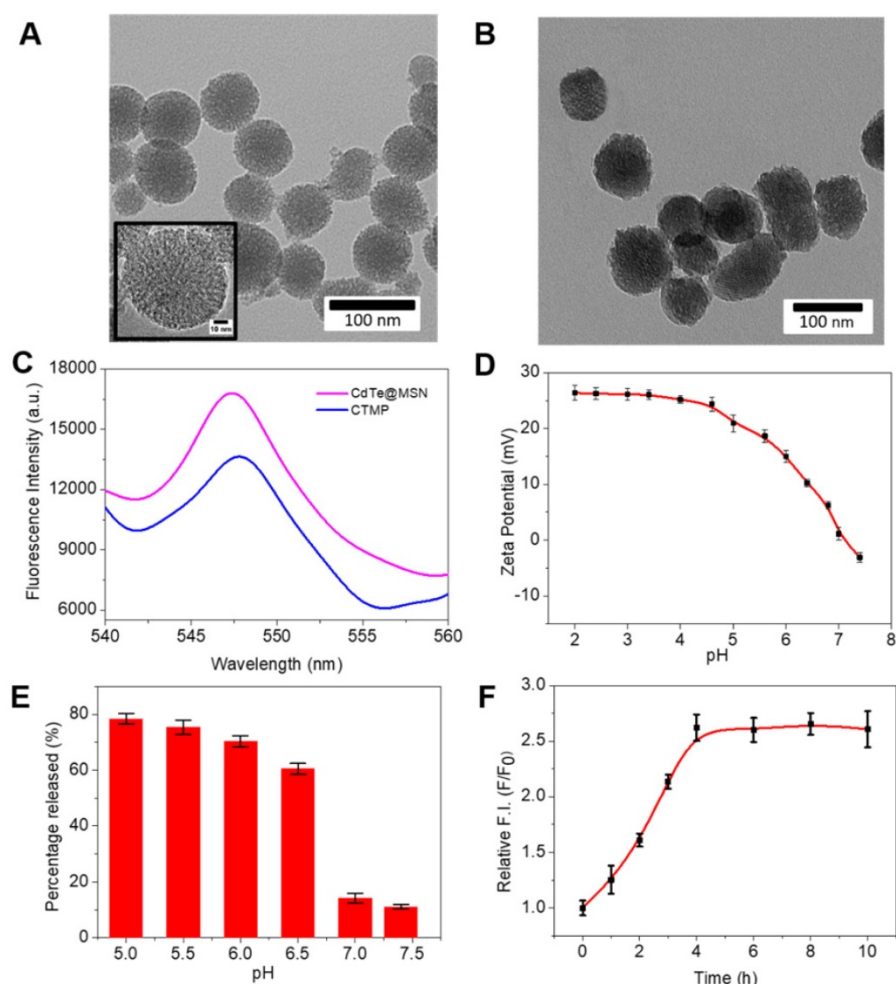


Figure 1. The TEM images of (A) CdTe@MSN and (B) CTMP. (C) The fluorescence spectra of CdTe@MSN (Pink) and CTMP (Blue) ($\lambda_{ex} = 488$ nm). (D) Zeta potential of the CTMP with various pH values from 2.0 to 7.4. (E) Percentage of AA released from CTMP-AA at different pH values within 24 h. (F) Fluorescence recovery of CTMP-AA with time.

For the next step, zeta potential titration experiments of the sample CTMP were carried out to prove the change of charge state of the polymers on the surface of CdTe@MSN (Figure 1D). The protonation of nitrogen atoms in the pyridines of the polymer structure under acidic conditions causes the polymer chains to repel each other and enhance the hydrophilicity to open the pores of the nanocarriers. As the pH of the solution increases to 7.4, the zeta potential of the nanocarrier gradually decreases from a higher positive value (+25 mV) to a more negative value (-5 mV), which corresponds to the deprotonation of the nitrogen atom in the polymer structure under basic conditions and enhanced hydrophobicity. Such changes further cause the crossover of the polymer chain and then close the pores. The change of the hydrophilicity state of the nanocarrier has a regulatory effect on the release of the drug (Scheme 1). It can be seen from Figure 1E that the release efficiency of the drug in the pH 6.0 buffer solution reaches 65% within 24 hours, but drops to 15% in the buffer solution with pH = 7.4. Hence, the as

synthesized nanocarriers are proved to be pH sensitive [37, 38], and own potential application in controlled reversible drug release.

Fluorescence Measurements of CTMP-AA

To further examine the nanocarriers' fluorescence change, the maximum loading of AA was tested and a significant quenching of CTMP-AA's was obtained (Figure S6). The fluorescence quenching effect attributes to the charge change on the nanocarriers' surface after AA loaded. Moreover, after the AA release, the fluorescence intensity of CTMP-AA recovered by approximately 2.5 times (Figure 1F), indicating that the interaction between nanocarriers and AA occupies a fluorescent response, which helps the nanocarriers' localization.

The CTMP's targeting ability towards HepG2 cells

To evaluate the targeting ability of the CTMP, the nanocarrier was used to analyze the HepG2 cells (human hepatocellular liver carcinoma cells) and

HL-7702 cells (human hepatocyte cells). Typically, HepG2 and HL-7702 cells were respectively incubated with CTMP for 4 h, where the green fluorescence intensity in HepG2 cells was much stronger than in HL-7702 cells (Figure S7), demonstrating the successful targeting of CTMP to HepG2 cells. Similar results were also obtained from the flow cytometry analysis (Figure S8) for verification. The fluorescence recovery of CTMP-AA in HepG2 cells was verified under the same concentration conditions, where cells were incubated for different time (0, 2, 4, 6 & 8 h) under hypoxia (1% O₂). As shown in Figure S9, the fluorescence recovery of the nanocarrier display significant change in the first 4 h, and then stays almost unchanged afterwards. The internal fluorescence intensity gradually increased with time, representing that CTMP-AA keep releasing AA inside of the cell. In addition, MTT assays were also used to explore the toxicity of different CTMP's concentrations, and over 90% cell viabilities were acquired to prove its great biocompatibility (Figure S10). In this regard, CTMP has excellent fluorescence imaging effect and can target HepG2 cells to improve drug delivery efficiency.

Comparison of NAD(P)H change caused by CTMP-AA

Recent studies found that AA can function as a versatile reducing agent in biological applications. NAD(P)H, as a reducing coenzyme in the process of cell metabolism *in vivo*, is an important indicator for characterizing intracellular reduction [39-41]. Hence, in order to compare the difference of NAD(P)H content caused by AA, the fluorescence signal intensity change in HepG2 cells with the NAD(P)H probe DCI-MQ was investigated [42]. Typically, HepG2 cells were incubated with CTMP-AA under hypoxia for different times variations (0, 2, 4, 6 and 8 h), and then the fluorescence intensity changes of DCI-MQ were acquired and quantified (Figure 2).

Notably, as CTMP-AA releases more AA to intracellular environment, the NAD(P)H content increases as well, leading to a gradual fluorescence enhancement till 6 h. Consequently, as the cell morphology exhibiting blurred at 8 h, which proves the release of AA further strengthen the degrees of reducing stress.

The influence of CTMP-AA on HepG2 cells' apoptosis

To further investigate the influence of CTMP-AA on cancer cells' apoptosis, the AnnexinV-FITC/PI Apoptosis Kit was applied to examine cell survival by flow cytometry. AnnexinV-FITC stained membrane displays green fluorescence, and the fluorescence intensity correlates with the pre-apoptotic state, while PI staining displays orange fluorescence and its imaging brightness correlates to the late stage of apoptosis (Figure S11). Compared with the control group at 0 h, the intracellular fluorescence intensity of the cell image brightens with time, indicating that the number of dead cells rises. The killing effect of CTMP-AA on HepG2 cells increases with time and maximizes at 8 h, which was considered as the most unbalanced redox environment in the cells.

The HepG2 and HL-7702 cells were respectively incubated with CTMP-AA, and then verified by MTT experiment and apoptosis kits. The HL-7702's survival rate under normoxia is higher than that of HepG2 cells under hypoxia, demonstrating the nanocarriers improve the efficiency of killing effect and drug delivery through targeting the HepG2 cells but avoid damaging normal cells (Figure S12). Annexin V-FITC/PI kit was then used to study the CTMP-AA's influence on HepG2 cell's apoptosis. Same concentration of CTMP, free DHA, free AA and CTMP-AA were respectively incubated with HepG2 cells for 8 h under hypoxia (1% O₂), and the apoptosis rate of HepG2 cells was measured by flow cytometry (Figure 3). Compared with the control group,

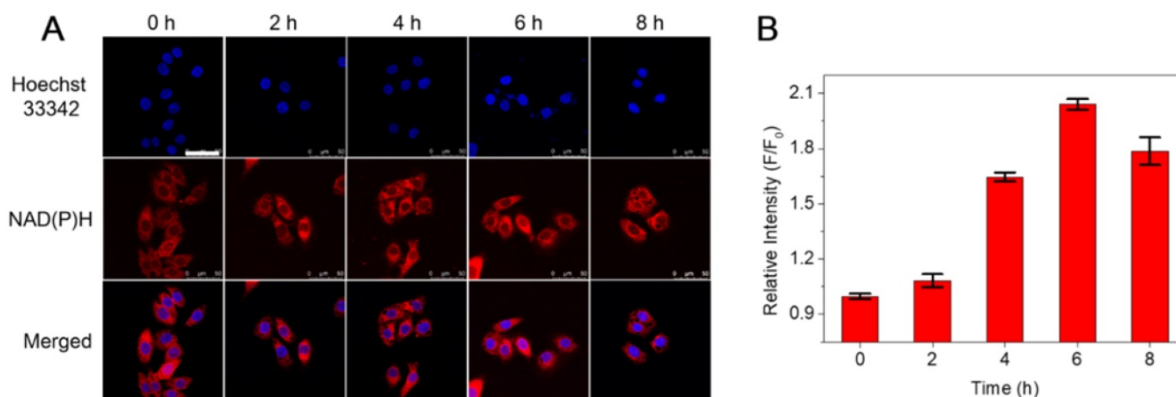


Figure 2. (A) Confocal fluorescence images of NAD(P)H in HepG2 cells incubated with CTMP-AA under hypoxia (1% O₂) for different times (0, 2, 4, 6 and 8 h). (B) The quantitative fluorescence intensities of results in (A). The nucleus was stained with Hoechst 33342. Scale bars are 50 μ m.

CTMP-AA exhibits best curative effect. Notably, the early and late apoptosis of the cells accounted for 17.2% and 23.5% respectively. Moreover, CTMP-AA improves drug delivery efficiency and avoids oxidation of free AA before it enters cells, thereby better induces apoptosis than others.

In vivo study

After the *in vitro* performance study of the CTMP-AA, it was then applied to the *in vivo* study via HepG2 cells inoculated mice for examine its therapeutic effect [43]. The mice were intravenously administered with 25 mg/kg CTMP-AA and fluorescence images were acquired after 24 h. Compared to the control group, a higher level of fluorescence intensity in the tumor tissues was obtained for the treated mouse (Figure 4A & 4B), indicating an excellent targeting effect during the delivery. Remarkably, the accumulated fluorescence mainly exhibit in the tumor site (Figure 4C & 4D), designates that CTMP-AA can target the tumor site of the nude mice. Moreover, the nanocarriers can also be excreted through the liver and kidneys, and then being metabolized to the outside of the body to avoid the toxic side effect in the long run.

In order to better investigate the nanocarriers' therapeutic effect, representative images of mice for 20 days treatment were taken (Figure 5A). According

to the tumor volume of each treatment group, CTMP-AA group displays a significant inhibition effect on the tumor growth (Figure 5B), which is caused by more delivered AA in CTMP to improve the curing efficacy. Comparison of the dissected tumors' weight in the mice of each treatment group also reaches the same conclusion (Figure 5C & S13). The mice in each group were stable in weight (Figure 5D), signifying that the treatment is safe *in vivo*. Moreover, from the HE staining of tumors and major organs in each treatment group (Figure S14), necrosis of tumor was obtained from the CTMP-AA group, which further verifies the curing effectiveness. In addition, no obvious damage in all organs was found, indicating CTMP-AA's safety and biocompatibility.

At the cellular level, we have demonstrated that CTMP-AA controlled release of AA leads to reductive stress-induced apoptosis in HepG2 cells. With hypoxic reducing environment, the tumor sites of both mice in Figure S15 display fluorescence response to the DCI-MQ probe. However, the CTMP-AA group shows significantly higher intensity than the control group, indicating a higher amount of NAD(P)H inside of the tumor. Hence, it can be concluded that AA can enter the tumor lesion area by CTMP, accumulate reducing species and enhance the reductive stress, thereby significantly inhibiting tumor growth.

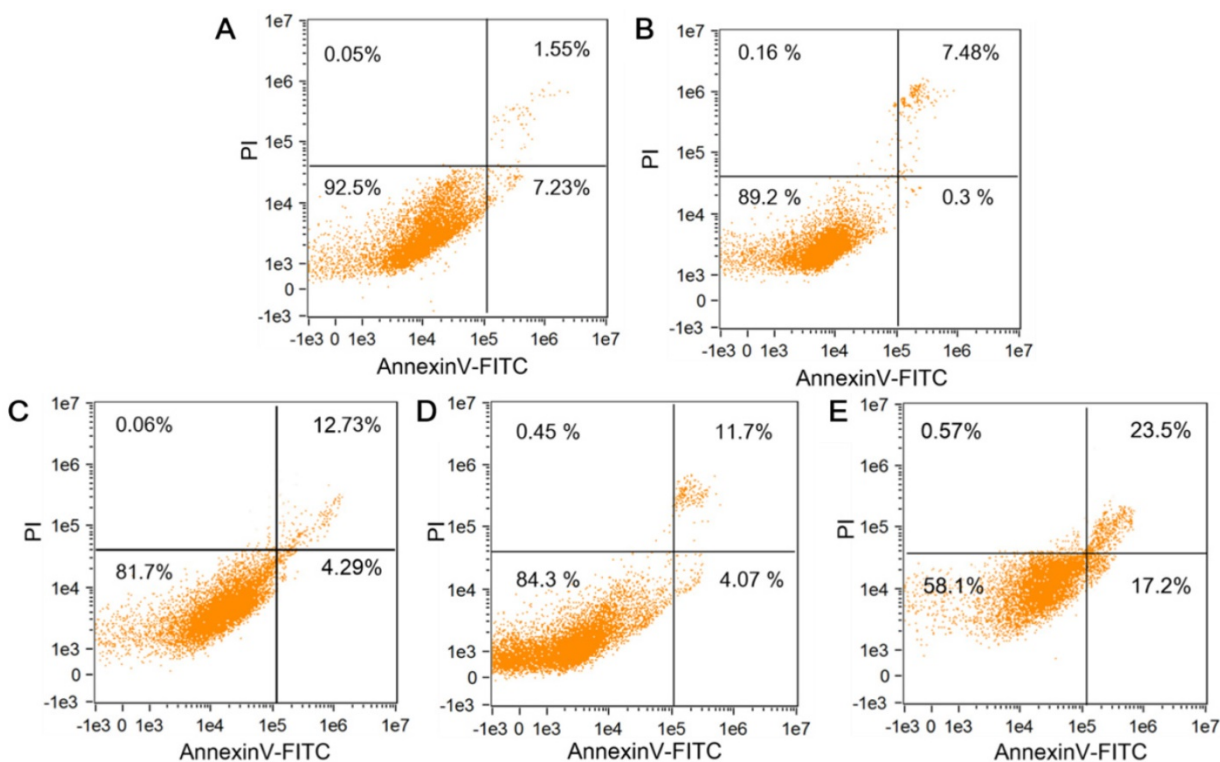


Figure 3. The flow cytometry analysis of cells' apoptosis following treatments with different reagents: (A) NS buffer, (B) CTMP, (C) Free DHA, (D) Free AA and (E) CTMP-AA.

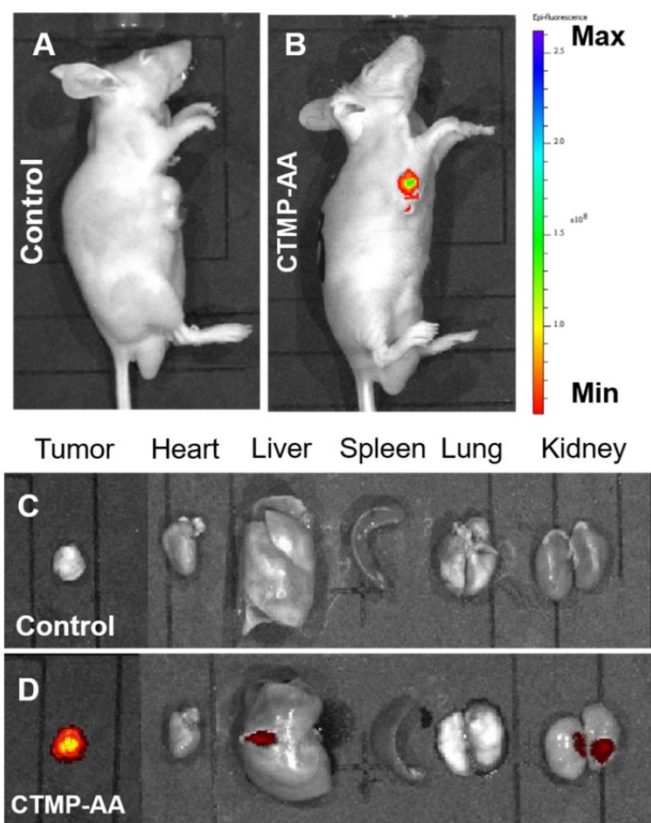


Figure 4. *In vivo* fluorescent imaging of HepG2 tumor-bearing mice which were intravenously injected with CTMP-AA after 24 h: (A) the control groups: 50 μ L normal saline; (B) the treatment groups: 25 mg/kg. (C) and (D) *Ex vivo* fluorescence images of major organs and tumors corresponds to (A) and (B).

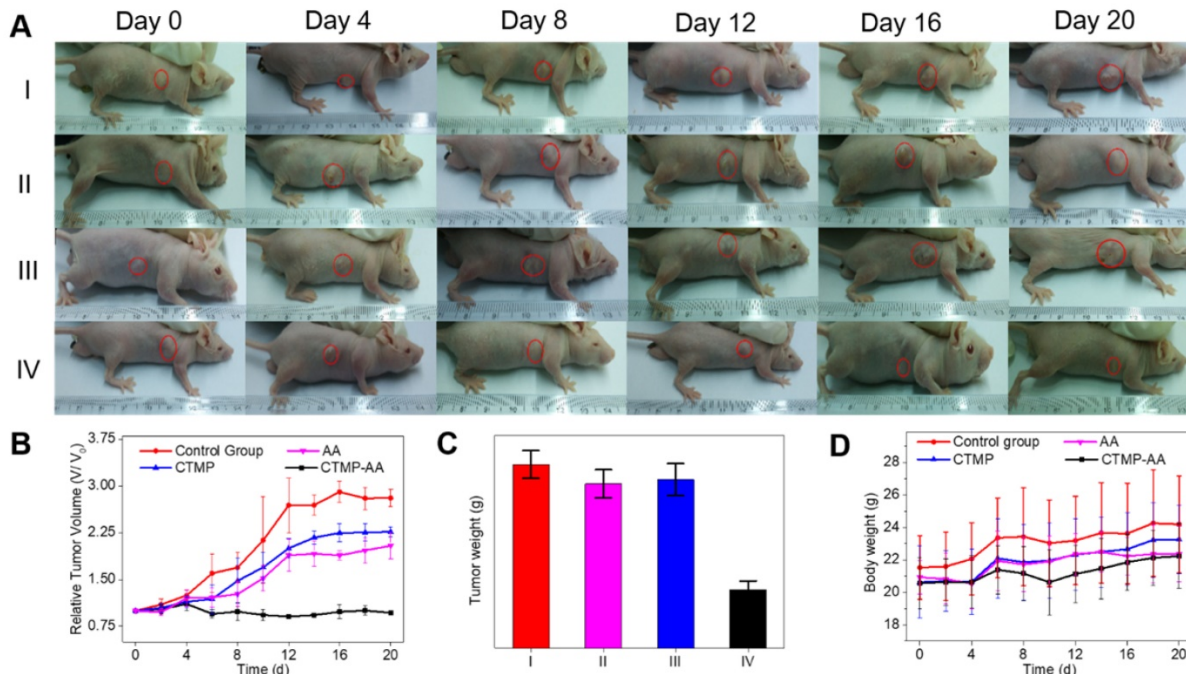


Figure 5. Antitumor effect of CTMP-AA: (A) the representative images of mice following 20-days treatment for each treatment group; (B) quantitative results of the HepG2 relative tumor volumes. Tumor volumes were normalized to their initial size. (C) Quantitative results of the tumors' weight: (I) Normal saline (NS) as the control group, (II) Free AA, (III) CTMP and (IV) CTMP-AA. (D) The mice weight changes for each treatment group. All data is shown as mean \pm S.D.; n = 5 per group.

Conclusions

In summary, a core-shell nanostructure of CdTe quantum dots with mesoporous silica coating was

developed and functionalized with PPF, which achieves cancer cells' targeting delivery and reversibly pH controlled release of AA both *in vitro* and *in vivo*. In the hypoxia acidic environment, AA

was found to enrich the reductive species, break the redox balance in HepG2 cells and trigger the reductive stress to induce the apoptotic signaling pathway. The *in vivo* study further verified CTMP-AA has a killing effect on tumor cells and inhibition of tumor growth, thereby achieving therapeutic effects. For the first time we proposed the concept for applying reductive stress into cancer treatments, which brings great advantage of toxicity free and less damage to normal tissues. In general, this technique has taken an important step in the development of a targeted tumor treatment system, providing perspectives for the design of medicines *via* reductive stress, and offers new insights into future clinical mild-therapies.

Experimental Section

Preparation of CdTe@MSN NPs

The CdTe@MSN NPs were synthesized according to the base-catalysed sol-gel method reported previously with further modifications. Typically, 5 mg of CdTe quantum dots (QDs), 0.2 g CTAB and 0.6 mL NaOH (2 M) solution were added into 100 mL H₂O under vigorous stirring to obtain the aqueous solution. The mixture was homogenized at 40 °C for 3 h to produce a uniform dispersion, and then TEOS (1 mL) and APS (0.2 mL) were introduced dropwisely to the solution, followed by adjusting the solution temperature to 80 °C. The mixture was allowed to stir for 3 h to yield light yellow precipitates (as synthesized CdTe@MSN-NH₂). The solid product was washed with ultrapure water and methanol (1:1), and then dried in vacuum. To remove the surfactant template (CTAB), 0.5 g as synthesized amino modified mesoporous silica was refluxed for 24 h in a solution of 3 mL of HCl (37.4%) and 50 mL of methanol, followed by extensive washes with ultrapure water and methanol. Finally, the precipitates were dried for 24 h in vacuum at room temperature.

Preparation of CTMP

The CTMP nanocarriers were obtained by the amide bond formation *via* coupling the carboxyl group of the PPF and the amino group from the surface of CdTe@MSN. 10 mg EDC and 10 mg sulfo-NHS and 14 mg PPF were added to 10 mL THF, and the mixture was reacted for 30 min at room temperature to activate the carboxylate groups. CdTe@MSN (10 mg) was added and then kept stirring the mixture at room temperature for 24 h in dark. Afterwards the nanocarriers were washed 3 times by centrifugation (14,000 rpm, 15 min) and re-dispersion with a mixture of EtOH-water 1:1 (1 mL).

Confocal Fluorescence Imaging

HepG2 and HL-7702 cells were seeded in 20 mm glass bottom dishes (5×10⁴ cells/dish) and incubated for 24 h, HepG2 and HL-7702 cells were respectively incubated with CTMP (100 µg/mL) for 4 h. After the nanoplatfrom incubation, the residual NPs were removed by washing with PBS buffer for three times, and the cell nuclei were stained with Hoechst 33342 before the CLSM imaging. The 405 nm excitation wavelength for Hoechst 33342, and 488 nm excitation wavelength for CTMP were employed.

CTMP-AA Induced HepG2 Cells' Apoptosis

In order to investigate the influence of CTMP on HepG2 cells' apoptosis, AnnexinV-FITC/PI apoptosis kit was applied. The HepG2 cells were cultured in 30 mm cell culture dishes for 24 h and then divided into 4 groups, and cultured for 8 h with CTMP, DHA, AA, CTMP-AA under hypoxia (1% O₂) respectively. The cells were trypsinized and collected by centrifugation (1,000 rpm, 5 min), followed by washing twice with PBS buffer solution. Consequently, 0.2 mL of Annexin buffer and 5 µL of FITC were added for 20 min incubation at room temperature. Finally, 300 µL of Annexin buffer and 10 µL PI were added for collecting cells that used for flow cytometry within 1 hour. The data was analyzed by IDEAS image analysis software. Another way applied to detect apoptosis is to calculate the survival rate of HepG2 cells by MTT assay.

Abbreviations

NADPH: nicotinamide adenine dinucleotide phosphate; AA: ascorbic acid; DHA: dehydroascorbic acid; PPF: poly(2-vinylpyridine)-polyethylene glycol-folic acid; TEM: transmission electronic microscopy; UV-Vis: UV-visible absorption spectroscopy; MSN: mesoporous silica nanoparticles; CTMP: CdTe@MSN@PPF; HRMS: high resolution mass spectrometry.

Supplementary Material

Supplementary methods and figures.
<http://www.thno.org/v09p4233s1.pdf>

Acknowledgements

This work was supported by National Natural Science Foundation of China (21535004, 91753111, 21575081, 21775091 and 21705098), the Key Research and Development Program of Shandong Province (2018YFJH0502), Natural Science Foundation of Shandong Province (ZR201702200428), Project of Shandong Province Higher Educational Science and Technology Program (J17KA116).

Competing Interests

The authors have declared that no competing interest exists.

References

- Fujimoto A, Totoki Y, et al. Whole-genome sequencing of liver cancers identifies etiological influences on mutation patterns and recurrent mutations in chromatin regulators. *Nat. Genet.* 2012; 44: 760-764.
- Kaiser J. Combining targeted drugs to stop resistant tumors. *Science.* 2011; 331: 1542-1545.
- Oh TY, Lee JS, et al. Oxidative damages are critical in pathogenesis of reflux esophagitis: implication of antioxidants in its treatment. *Free Radical Biol. Med.* 2001; 30: 905-915.
- Fan H, Yan G, et al. A smart photosensitizer-manganese dioxide nanosystem for enhanced photodynamic therapy by reducing glutathione levels in cancer cells. *Angew. Chem. Int. Ed.* 2016; 55: 5477-5482.
- Zhao Z, Meng H, et al. A controlled-release nanocarrier with extracellular pH value driven tumor targeting and translocation for drug Delivery. *Angew. Chem.* 2013; 125: 7635-7639.
- Han H, Jin Q, et al. The rational design of a gemcitabine prodrug with AIE-based intracellular light-up characteristics for selective suppression of pancreatic cancer cells. *Chem. Commun.* 2015; 51: 17435-17438.
- Li, Y, Sun Y, et al. Ultrasensitive near-infrared fluorescence-enhanced probe for in vivo nitroreductase imaging. *J. Am. Chem. Soc.* 2015; 137: 6407-6416.
- Zhao Y, Hu Q, et al. SoNar, a highly responsive NAD⁺/NADH sensor, allows high-throughput metabolic screening of anti-tumor agents. *Cell Metab.* 2015; 21: 777-789.
- Xiao X, Li Y, et al. Small-molecule fluorescent probes for imaging and detection of reactive oxygen, nitrogen, and sulfur species in biological systems. *Anal. Chem.* 2018; 90: 533-555.
- Shenoy N, Creagan E, et al. Ascorbic acid in cancer treatment: let the phoenix fly. *Cancer Cell.* 2018; 34: 700-706.
- Veech RL, Guynn R, et al. The time-course of the effects of ethanol on the redox and phosphorylation states of rat liver. *Biochem. J.* 1972; 127: 387-397.
- Pan X, Song X, et al. H₂Se induces reductive stress in HepG2 cells and activates cell autophagy by regulating the redox of HMGB1 protein under hypoxia. *Theranostics.* 2019; 9(6): 1794-1808.
- Kong F, Ge L, et al. A highly selective near-infrared fluorescent probe for imaging H₂Se in living cells and *in vivo*. *Chem. Sci.* 2016; 7: 1051-1056.
- Lu T, Pan Y, et al. Gene regulation and DNA damage in the ageing human brain. *Nature.* 2004; 429: 883-891.
- Rajasekaran NS, Connell P, et al. Human α B-crystallin mutation causes oxido-reductive stress and protein aggregation cardiomyopathy in mice. *Cell.* 2007; 130: 427-439.
- Cheng R, Kong F, et al. Simultaneous detection of mitochondrial hydrogen selenide and superoxide anion in HepG2 cells under hypoxic conditions. *Anal. Chem.* 2018; 90: 8116-8122.
- Chen T, Wong YS, et al. Selenocystine induces reactive oxygen species-mediated apoptosis in human cancer cells. *Biomed. Pharmacother.* 2009; 63: 105-113.
- Song JH, Shin SH, et al. Involvement of oxidative stress in ascorbate-induced proapoptotic death of PC12 cells. *Exp. Neurol.* 2001; 169: 425-437.
- A. Chakraborty, N. R. Jana, Vitamin C-conjugated nanoparticle protects cells from oxidative stress at low doses but induces oxidative stress and cell death at high doses. *ACS Appl. Mater. Interfaces.* 2017; 9: 41807-41817.
- Q. Chen, M. G. Espey, et al. Pharmacologic ascorbic acid concentrations selectively kill cancer cells: Action as a pro-drug to deliver hydrogen peroxide to tissues. *Proc. Natl. Acad. Sci. U. S. A.* 2005; 102: 13604-13609.
- Q. Chen, M. G. Espey, et al. Ascorbate in pharmacologic concentrations selectively generates ascorbate radical and hydrogen peroxide in extracellular fluid *in vivo*. *Proc. Natl. Acad. Sci. U. S. A.* 2007; 104: 8749-8754.
- Gonçalves AC, Alves V, et al. Oxidative stress mediates apoptotic effects of ascorbate and dehydroascorbate in human Myelodysplasia cells *in vitro*. *Toxicol. In Vitro.* 2013; 27: 1542-1549.
- Matsuoka Y, Yamato M, et al. Fluorescence probe for the convenient and sensitive detection of ascorbic acid. *J. Clin. Biochem. Nutr.* 2016; 58: 16-22.
- Packer JE, Slater TF, et al. Direct observation of a free radical interaction between vitamin E and vitamin C. *Nature.* 1979, 278: 737-738.
- Yun J, Mullarky E, et al. Vitamin C selectively kills KRAS and BRAF mutant colorectal cancer cells by targeting GAPDH. *Science.* 2015; 350: 1391-1396.
- Xu K, Wang F, et al. High selectivity imaging of nitroreductase using a near-infrared fluorescence probe in hypoxic tumor. *Chem. Commun.* 2013; 49: 2554-2556.
- Roberts NJ, Zhang L, et al. Intratumoral injection of Clostridium novyi-NT spores induces antitumor responses. *Sci. Transl. Med.* 2014; 6: 249ra111.
- Zheng X, Mao H, et al. Successively activatable ultrasensitive probe for imaging tumour acidity and hypoxia. *Nat. Biomed. Eng.* 2017; 1: 0057.
- Chang B, Zhang X, et al. General one-pot strategy to prepare multifunctional nanocomposites with hydrophilic colloidal nanoparticles core/mesoporous silica shell structure. *J. Colloid Interface Sci.* 2012; 377: 64-75.
- Li DY, Qin YP, et al. A "turn-on" fluorescent receptor for detecting tyrosine phosphopeptide using the surface imprinting procedure and the epitope approach. *Biosens Bioelectron.* 2015; 66: 224-230.
- Chen H, Wang J, et al. Dual-emitting fluorescent metal-organic framework nanocomposites as a broad-range pH sensor for fluorescence imaging. *Anal. Chem.* 2018; 90: 7056-7063.
- Wang J, Chen H, et al. Encapsulation of dual-emitting fluorescent magnetic nanoprobe in metal-organic frameworks for ultrasensitive ratiometric detection of Cu²⁺. *Chem. Eur.* 2018; 24: 3499-3505.
- Liu JN, Bu WB, et al. Silica coated upconversion nanoparticles: a versatile platform for the development of efficient theranostics. *Acc. Chem. Res.* 2015; 48: 1797-1805.
- Niedermayer S, Weiss V, et al. Multifunctional polymer-capped mesoporous silica nanoparticles for pH-responsive targeted drug delivery. *Nanoscale.* 2015; 7: 7953-7964.
- Gao W, Cao W, et al. AuNP flares-capped mesoporous silica nanoplatform for MTH1 detection and inhibition. *Biomaterials.* 2015; 69: 212-221.
- Ma Q, Yu W, et al. Detection of newcastle disease virus with quantum dots-resonance light scattering system. *Talanta.* 2010; 82: 51-55.
- Mei X, Chen D, et al. Hollow mesoporous silica nanoparticles conjugated with pH-sensitive amphiphilic diblock polymer for controlled drug release. *Microporous Mesoporous Mater.* 2012; 152: 16-24.
- Muhammad F, Guo M, et al. pH-triggered controlled drug release from mesoporous silica nanoparticles via intracellular dissolution of ZnO nanolids. *J. Am. Chem. Soc.* 2011; 133: 8778-8781.
- Brewer AC, Mustafi SB, et al. Reductive stress linked to small HSPs, G6PD, and Nrf2 pathways in heart disease. *Antioxid. Redox Sign.* 2013; 18: 1114-1127.
- Dimmeler, Stefanie Zeiher, Andreas M. A "reductionist" view of cardiomyopathy. *Cell.* 2007; 130: 401-402.
- Yin P, Hung, John G. Albeck, M. Tantama and G. Yellen. Imaging cytosolic NADH-NAD⁺ redox state with a genetically encoded fluorescent biosensor. *Cell Metab.* 2011; 14: 545-554.
- Zhao Y, Wei K, et al. Dicyanoisophorone-based near-infrared-emission fluorescent probe for detecting NAD (P) H in living cells and *in vivo*. *Anal. Chem.* 2018; 91: 1368-1374.
- Yu Z, Ge Y, et al. A pre-protective strategy for precise tumor targeting and efficient photodynamic therapy with a switchable DNA/upconversion nanocomposite. *Chem. Sci.* 2018; 9: 3563-3569.